- Technical Paper -

VISUALIZATION OF CORRODED STEEL BARS IN RC BEAMS USING DIGITAL IMAGE PROCESSING OF X-RAY PHOTOGRAMS

Sopokhem LIM[*1], Haitao JIANG[*2], Takehiro OKAMOTO[*3] and Mitsuyoshi AKIYAMA[*4]

ABSTRACT

The structural performance of deteriorated RC structures in chloride-contaminated environments depends strongly on local conditions of corrosion-damage reinforcement. Corrosion-induced surface cracking is the only key visible indicator that indicates steel corrosion inside RC members. Therefore, it is crucial to study the spatial variability of steel weight loss in relation to corrosion cracking. This paper demonstrates applications of X-ray techniques and digital image processing to continuously observe the spatial variation of steel weight loss and its relationship with surface crack widths.

Keywords: RC beam, spatial variability, steel weight loss, surface crack width, X-ray technique, digital image processing

1. INTRODUCTION

Chloride-induced steel corrosion is a major cause of deterioration of RC structures in marine environments. Gradual ingress of chloride attack on RC members over time damages protected concrete covers. Once chloride reaches the reinforcement surface, steel corrosion begins. Because the product of steel corrosion occupies a greater volume than the original reinforcing bar, it induces cracks in the concrete cover and subsequently surface cracks. In previous studies [1] & [2], propagation and widening time of bending and longitudinal surface cracks were reported to be longer than the corrosion-induced cracking time. The loss of steel bar cross-sectional area, which was associated with the crack width, did not substantially affect the ultimate state but did affect the serviceability state. Consequently, deteriorated RC structures represent a considerable economic loss in terms of maintenance and repair work. Therefore, the reliable prediction of the long-term performance of deteriorated existing RC structures is required for on-time maintenance and rehabilitation.

Recently, efforts based on probabilistic concepts and methods have been made to estimate the long-term structural performance of deteriorated RC members. However, limited amounts of experimental data on the spatial variation of steel weight loss in relation to surface crack widths have been reported, creating difficulties in improving the degree of accuracy associated with prediction models [3].

The scarcity of experimental data is due to the difficulty in studying the non-uniform distribution of steel weight loss in relation to crack widths at various stages of corrosion. Although it is possible to use the common destructive method by repeatedly breaking specimens to weigh the steel bar at various stages of corrosion, this method is inefficient and error-prone due to difficulties in making experimental conditions repeatable and uncertainties in the specimens used, particularly with respect to growth patterns and measurements of the crack widths.

To avoid these problems, X-ray technique can be used as a better option because it is a non-destructive method that enables a continuous investigation of corroded steel bars throughout the corrosion process. Presently, there have only been a few experimental studies that employ the X-ray technique to investigate steel corrosion. Beck et al. [4] examined the surface of a small steel cylinder (9 mm in diameter and 10 mm long) inside a mortar specimen at various stages of corrosion using X-ray computer tomography. In this experiment, it was found that the mass loss estimated by the constructed 3-D image was different by 40-60% from the actual measured mass loss after breaking the specimen. Akiyama and Frangopol [5] proved that the X-ray apparatus was a suitable tool for a continuous investigation of a corroded steel bar in a concrete cylinder (100 mm × 200 mm) and prism (100 mm × 100 mm × 400 mm). The weight loss of a steel bar was estimated by a digital image analysis of X-ray photograms of a corroded steel bar from different viewing angles. The estimated steel weight loss using photograms was found to be different by only 10% from that measured by weight after damaging the specimen.

The primary objective of this paper is to experimentally investigate the continuous growth of the spatial distribution of steel weight loss along a corroded steel bar inside a RC beam using digital image

*1 Graduate School of Creative Sciences and Engineering, Waseda University, JCI Student Member
*2 Graduate School of Creative Sciences and Engineering, Waseda University
*3 Graduate School of Creative Sciences and Engineering, Waseda University
*4 Professor, Dept. of Civil and Environmental Engineering, Waseda University, JCI member

processing of X-ray photograms. The relationship between the steel weight loss and corresponding surface crack widths is also discussed. Although the experimental technique in the study is adapted from [5], larger specimens with longer lengths of corroded steel bars are to be investigated. Using a new upgraded X-ray apparatus and image intensifier, X-ray photograms can be acquired with a higher resolution that can detect corrosion products. The more advanced digital image analyzer also improves the accuracy of determining the steel weight loss. Since it is necessary to consider the spatial variability of steel weight loss in a prediction model for long-term structural performance of corrosion-affected RC structures, the outcome of the experiment is expected to be used together with corrosion levels assessed via in-situ inspections as input data to formulate a reliability prediction model. It can also be used to validate analytical estimation models of non-uniform steel weight loss.

2. TEST PROGRAMS

2.1 Material

(1) Reinforcing materials

A deformed bar with a diameter of 13 mm was used as a longitudinal bar, whereas deformed bars with a diameter of 6 mm were used as stirrups. All steel bars have the same steel grade SD345.

(2) Concrete

The concrete used had a 28-day compressive strength of 35 MPa. The ordinary Portland cement had a specific density of 3.15 g/cm^3. The fine aggregate having a fineness modulus of 2.60 and a specific density of 2.60 g/m^3 was used. The coarse aggregate used had a maximum size of 20 mm ($G_{max} \leq 20$ mm) and a specific density of 2.64 g/cm^3. The concrete mixing proportion by weight was as follows: cement:sand:gravel:water-to-cement (W/C) ratio = 1:2.08:2.65:0.5.

2.2 Test specimens

One RC beam with a tensile reinforcing steel bar and stirrups was used in the experiments. The specimen was 1,460 mm long with the cross section of 80×140 mm. The stirrups were arranged in intervals of 100 mm at its shear span. The details of the specimen are shown in Figure 1.

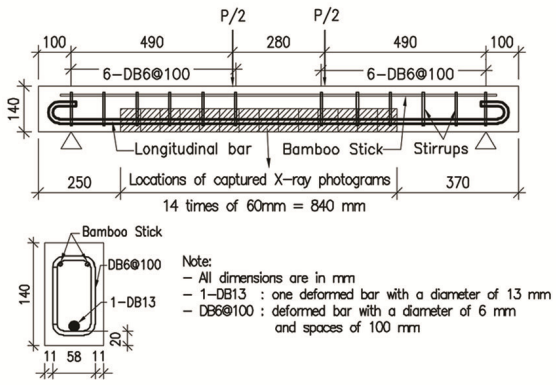

Fig. 1 Details of test specimen

To exclude the corrosion effect of the stirrups, they were wrapped with plastic tape to prevent direct contact with the longitudinal bar. Two days after fabrication, the specimen mold was stripped off and cured in a curing room at 23-25ºC for 28 days.

2.3 Experimental procedure

(1) X-ray photogram acquisition

Once before steel corrosion and several times during the corrosion process, photograms of the non-corroded and corroded steel bars inside the specimen were taken from different viewing angles using the X-ray configuration shown in Figure 2. The total length of the longitudinal steel bar to be visualized and captured was 840 mm, which required 14 times of continuously capturing 60-mm images along the steel bar, as shown in Figure 1. Images of the steel bar from viewing angles equal to 0°, 30°, 90°, 150°, 180°, 210°, 270°, and 330° were taken. The procedure of X-ray image acquisition consisted of two primary steps.

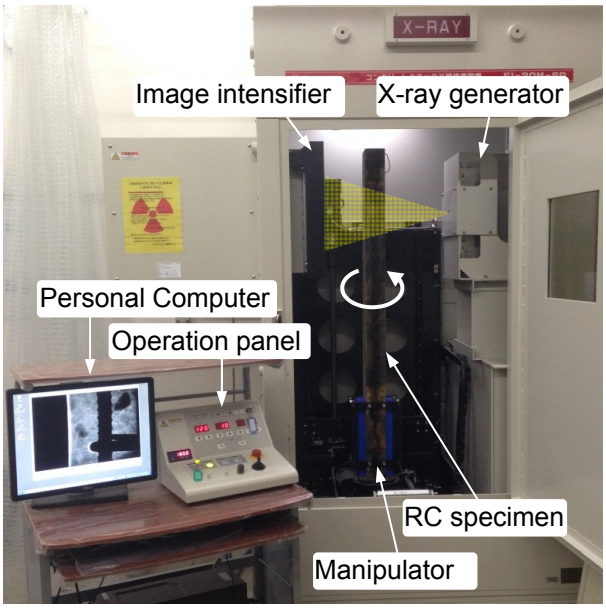

Fig. 2 X-ray configuration used to acquire photograms.

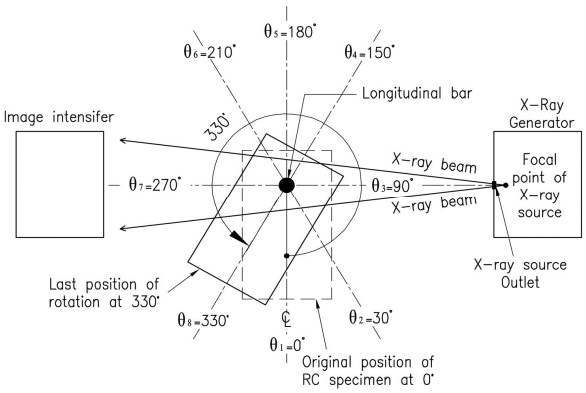

Fig. 3 Viewing angles used to capture photograms

The first step was setting up the specimen. The specimen was placed onto a manipulator between the image intensifier and X-ray generator in the X-ray

chamber. It was then adjusted horizontally to make the center of the embedded steel bar aligned with the middle point of the X-ray source outlet so that the longitudinal steel bar was fixed as a central point for the rotation of the specimen as shown in Figure 3.

After the setup, radiography image acquisition began by attenuating the primary X-ray beam with materials of different densities and thicknesses. The chosen X-ray power and current depended on different source-to-specimen distances and concrete thicknesses when the specimen was rotated to different viewing angles (i.e., 120 kV and 1.2 mA for 0°, 30°, 150°, 180°, 210°, and 330°, and 145 kV and 1.2 mA for 90° and 270°). Starting from a known position at 370 mm from the base of the specimen at a viewing angle of θ1 = 0°, the RC specimen was translated vertically with an increment of 60 mm 14 times against the radiation's cone beam. The acquired photogram was captured as an 8-bit grey-scale image with a size of 1024 × 768 pixels. The same process was implemented as the specimen was rotated to other angles (i.e., θ2, θ3, θ4, θ5, θ6, θ7, and θ8), as shown in Figure 3.

(2) Accelerated corrosion technique

After the curing of the specimen was complete at day 28, accelerated corrosion of the longitudinal steel bar was initiated during an electrochemical experimental test. The details of the test assembly are shown in Figure 4. The RC specimen was partially immersed in a 3% sodium chloride (NaCl) solution in a tank in a controlled environment at 23-25ºC. The external copper plate underneath the two pieces of wood supporting the specimen served as a cathode, whereas the embedded longitudinal bar in the specimen served as an anode. The applied direct current was adjusted for each specimen to maintain a current density of 1,000 μA/cm2 over the surface of steel bar. The accelerated corrosion process was continued until the steel weight loss reached approximately 10%.

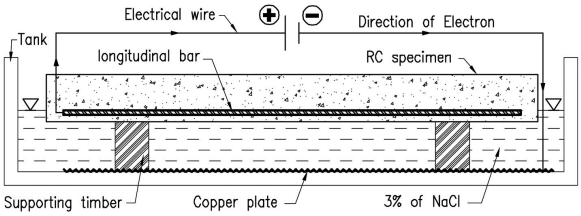

Fig. 4 electrochemical test assembly.

(3) External crack width

At various steel weight losses before X-ray radiography was performed, photographs of the longitudinal surface cracks were taken along the bottom of the specimen. The locations where these photographs were taken corresponded to those where the X-ray photograms were captured, as shown in Figure 1. 17 photographs, each of which was 50 mm long, were taken continuously along the bottom of the specimen. Crack width measurements using the photographs were continuously performed every 5 mm along the total length of 1,090 mm using an advanced image analysis program.

3. DIGITAL IMAGE PROCESSING OF X-RAY PHOTOGRAMS

3.1 Image Enhancement

The original X-ray photograms before enhancement of the non-corroded steel bar at different viewing angles are shown in Figure 5. In general, the images at 0° and 180° provided the clearest views, followed by images at 30°, 150°, 210°, and 330°; the worst images were found to be at angles of 90° and 270°. These results occurred due to the differences in the concrete thickness through which the X-ray radiation penetrated as the specimen was rotated to a particular angle (see Figure 3). For example, at 0° and 180°, the specimen was in a favorable position where the beam of X-rays penetrated through the concrete of 80 mm thick, producing notably clearer images. At 90° and 270°, the specimen was in position where the X-ray radiation had to penetrate 140 mm of concrete, producing the worst images. Moreover, even if the images at the viewing angle 0° provided the clearest views, it was difficult to scrutinize the evolution of the decayed shape and corrosion product of the corroded steel bar (see Figures 6a-d).

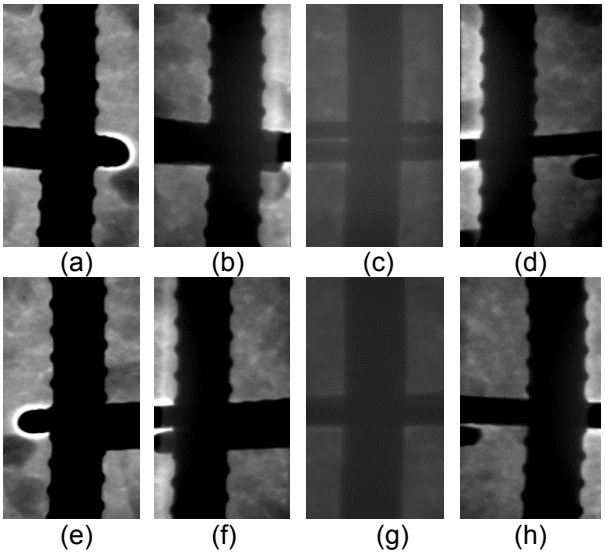

Fig. 5 (a)-(h) X-ray photograms of the original steel bar taken from viewing angles 0°, 30°, 90°, 150°, 180°, 210°, 270°, and 330°, respectively.

Therefore, it was necessary to enhance the images before analysis so that detailed information in the images could be easily manipulated and identified. The growth process of the corroded steel bar with increasing mean weight loss (hereafter denoted as *MSW*) from 0% to 2.60% to 6.03% to 8.77% could be seen more clearly with the enhanced images in Figures 6a1-d1 than those of original images in Figures 6a-d. Compared with the condition of the original steel bar in Figure 6a1, the decayed shape of the longitudinal steel bar could be detected near the stirrup in Figure 6b1 while the increase in corrosion product was observed in Figures 6c1 and 6d1.

In the enhancing process, the fine details of the image were revealed or the blurred regions were

reduced using a convolution filtering technique to accentuate intensity changes and make the high-contrast edge of the steel bar visible. The high-contrast edge was important for area segmentation between the steel bar and concrete during the digital image analysis to estimate the weight loss accurately.

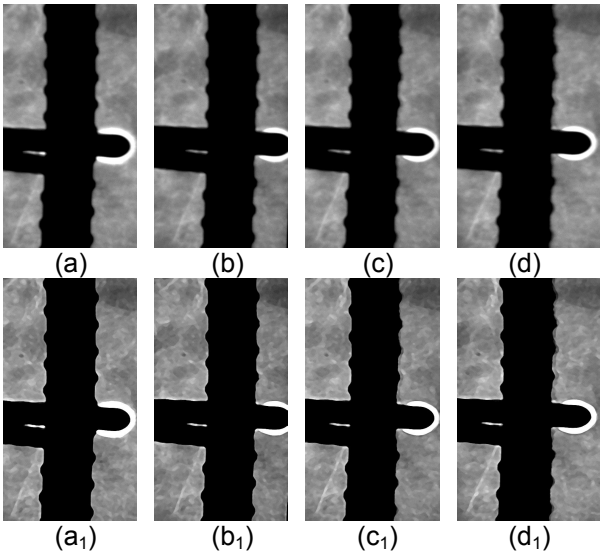

Fig. 6 X-ray photograms of developed stages of steel corrosion at 0° (a)-(d) before enhancement and (a_1)-(d_1) after enhancement as *MSW* increased from 0%, 2.60%, 6.03%, to 8.77%.

3.2 Steel weight loss estimation using X-ray photograms

To estimate the weight loss of the steel bar using the X-ray photograms, the areas of the original steel bar before corrosion and the corroded steel bar at a given time during the corrosion process must first be determined. The meaning of analyzing the digital images to determine an area of an object on the image (e.g., the steel bar area) is to manipulate the stored digital data on the image in terms of the numerical representation of pixels.

The X-ray photograms obtained in this study are 8-bit grey-scale images that consisted of 256 intensity values. These intensity values are the numeric representation of the grayness of the pixels on the image, which range from 0 for completely black to 255 for completely white. Because the reinforcing steel bar has a larger density than the concrete composite and corrosion product, it can absorb the X-ray radiation most efficiently. Therefore, the reinforcing steel bar always produces darker pixels with far lower intensities than the concrete composite and corrosion products do on the images. In Figures 7a-c, the intensity profile lines illustrate the intensity values along a row of pixels; this row of pixels corresponds to a line drawn on each of the above X-ray photograms. All profile lines show that the intensity values of the steel bar at 0°, 30°, and 90° in the middle part of each graph are always in ranges lower than those of corrosion products close to the corroded steel bar and the concrete composite in the left and right sides of the graphs. This is also applied to images of the remaining viewing angles because the images at 0° and 180°; 30°, 150°, 210°, and 330°; and 90° and 270° are similar (see Figure 5).

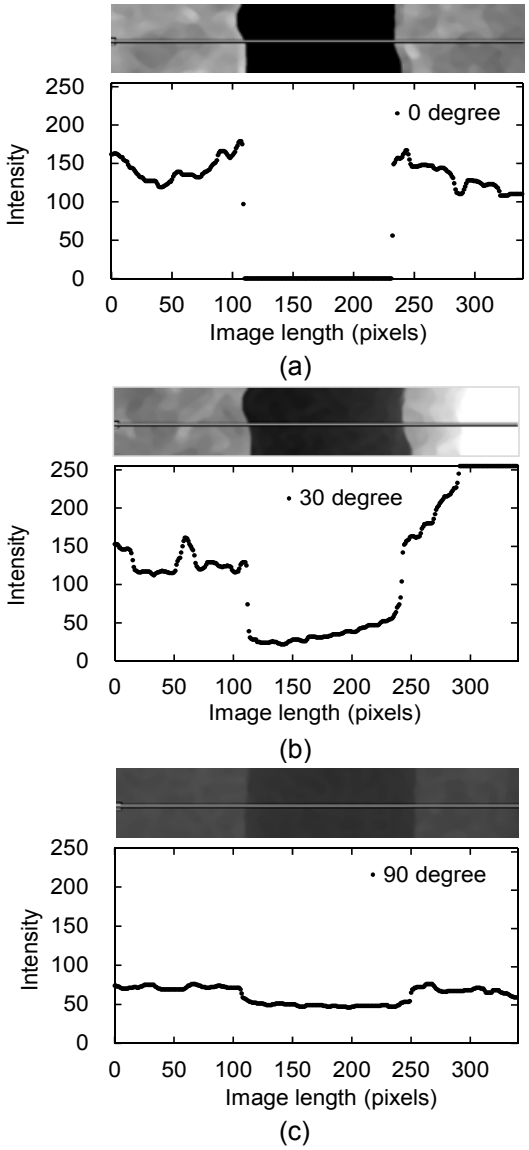

Fig. 7 (a), (b), and (c) Intensity profile lines of a row of pixels on the photograms of a corroded steel bar (*MSW* = 6.03%) at 0°, 30°, and 90°, respectively.

Therefore, by manipulating the numerical presentation of the pixels, it is possible to select the steel bar area by specifying a lower intensity threshold that belongs to only the pixels of the steel bar and count the number of pixels contained in that area. The histogram analyses in Figures 9a and 9b illustrate the cumulative number of pixels, which are classified according to the intensity values for the 5 mm long images of the non-corroded and corroded steel bars in Figures 8a and 8b, respectively. As explicitly indicated in Figures 9a and 9b, the total numbers of pixels (e.g., 8732 and 8449) are obtained by counting the cumulative number of pixels in the thresholds of the intensity value ranges of 0-57 and 0-58, which represent the area of the non-corroded and corroded steel bars in Figures 8a and 8b, respectively.

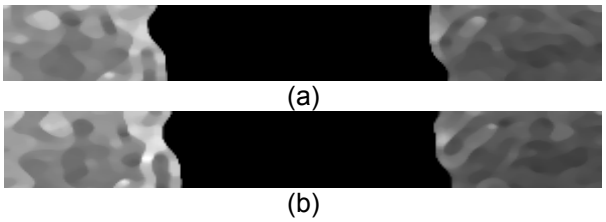

Fig. 8 Sliced 5-mm-long X-ray images at 0°, (a) an original bar and (b) a corroded bar (*MSW* =6.03%).

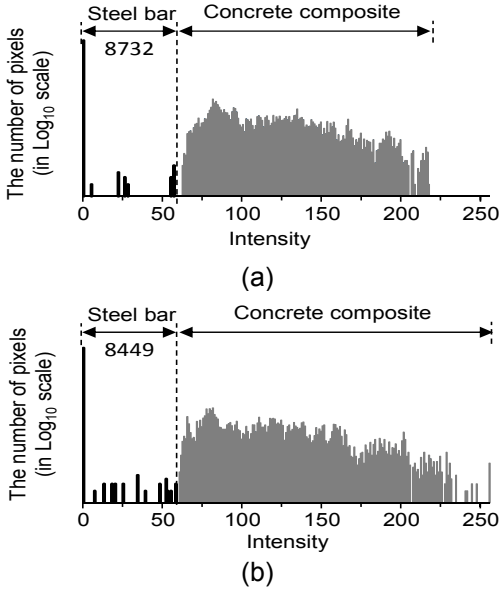

Fig. 9 Histograms of accumulative pixels classified according to the intensity values for (a) an original bar and (b) a corroded bar (*MSW* = 6.03%).

Once the areas of the original and corroded steel bars at each viewing angle are estimated using digital image processing of X-ray images, the steel weight loss per length L (mm) can be calculated by averaging the steel weight loss per length L from all viewing angles:

$$SW = \frac{1}{k}\sum_{n=1}^{k}\frac{(W_{\theta n} - SW'_{\theta n})}{W_{\theta n}} \times 100 \qquad (1)$$

where

SW : local steel weight loss per length L

$W_{\theta n}$: steel weight per length L estimated from an original steel area on a X-ray image at each viewing angle

$SW'_{\theta n}$: steel weight per length L estimated from a corroded steel area on a X-ray image at each viewing angle

θ_n : viewing angles (n = 1,..,k)

k : number of viewing angles

Regarding the accuracy in estimating the steel weight loss, it was already presented in [5]. Since the more updated X-ray apparatus, image intensifier, and image processing was used in this study, the accuracy is believed to be higher than that of [5].

4. RESULTS AND DISCUSSIONS

4.1 Spatial distribution of steel weight loss and corrosion-induced surface crack widths

The graph in Figure 10a shows the spatial distribution of the steel weight loss along the longitudinal steel bar and the associated surface cracks along the specimen length at *MSW* values of 0.68%, 2.60%, 6.03%, and 8.77%, respectively. Note that because the data of *SW* could not be obtained from the photograms at the locations where the stirrups were arranged at the shear span, there are regular gaps of some small portions of the line in the graph from 250 mm to 610 mm and from 850 mm to 1090 mm.

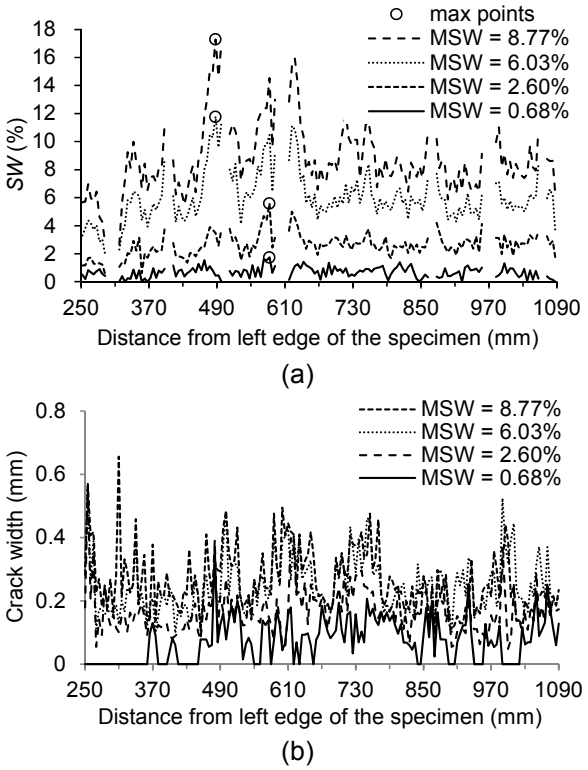

Fig. 10 Spatial distribution of (a) steel weight loss and (b) surface crack widths along the bottom specimen length (note: surface crack occurring only on the bottom surface of specimen).

In general, it can be seen from the graph that the distribution of steel weight loss is, as expected, spatially non-uniform because the *SW* values fluctuate in an erratic manner along the specimen length. The non-uniform degree of *SW* seems insignificant at the relatively low *MSW* of 0.68% but becomes increasingly volatile as the *MSW* increases from 2.60% to 6.03% to 8.77%. This result is reasonable because at the low *MSW* of 0.68%, not all cracks occur on the surface (see Figure 10) and thus may have a minor effect on the *SW* acceleration. As the *MSW* increases, the growing surface crack widths contribute more significantly to the acceleration of *SW,* which may make the non-uniform degree of *SW* become more rigorous. Based on locations, the non-uniform degree of the *SW* distribution seems to be more pronounced in the interval of the shear span (i.e., from 250 mm to 610 mm and from 870 mm to 1090 mm) than that of the constant-moment region (i.e., from 670 mm to 870 mm). For a detailed observation, several maximum *SW*, indicated by circles on the graphs, and several other

peaks of *SW* in the shear span that exacerbate the degree of variability most often occur near to the locations of the stirrups where small portions of the lines disappeared in the graph. This may be because the concrete covers at the locations of the stirrups are thinner than those at other locations, which may expose the longitudinal bar close to the stirrups to chloride and thus cause it to corrode relatively more quickly than the corroded steel at any other locations.

Furthermore, it is interesting to learn that the locations of maximum steel weight loss vary depending on the values of *MSW*. As indicated by some of the circles in the graph (i.e., maximum *SW* locations), the maximum steel weight loss is located at approximately 580 mm at the *MSW* of 0.68% and 2.60% but then shifts to approximately 490 mm at the *MSW* of 6.03% and 8.77%. This shift is likely to be caused by the shift in locations of the maximum corrosion crack widths at different amounts of steel weight loss or by some other uncertainties. With the experimental results of only one specimen, it is difficult to tell exactly about what causes this shift. Further extensive experimental studies that examine more parameters are required for future investigations.

On the other hands, the comparison between both graphs in Figures 10a and 10b show some peaks of steel weight loss and corrosion surface cracks occur approximately at the same locations of 490 mm, 610 mm, 730 mm, and 1000 mm. This shows the influence of steel weight loss to induce cracks in concrete covers at corresponded locations along the specimen.

4.2 Relationship between steel weight loss and surface crack widths

The graph in Figure 11 shows the relationship between the steel weight loss and the surface crack widths at their corresponding locations. It can be seen that the scattered points become more dispersed as the *MSW* increases. This indicates that the relationship between these two parameters weakens at higher amounts of *MSW*. Moreover, the relationship is observed not to start from the origin since some values of the crack widths are positive while those of *SW* are zero for the *MSW* = 0.68%. These minor errors might be caused by inaccurate measuring areas of the corroded bar at some locations on the images when the steel bar just started to corrode.

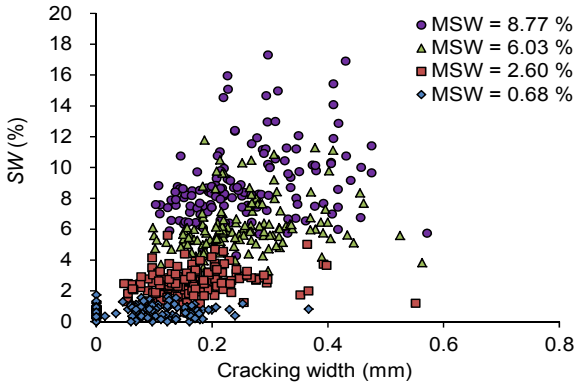

Fig. 11 Relationship between the steel weight loss and surface crack widths.

However, a positive trend is shown, where crack widths tend to increase with the increase in steel weight loss. This result demonstrates a possible relationship can be established between the two parameters.

5. CONCLUSIONS

In this paper, the procedure of using the X-ray technique to inspect a continuous spatial growth of a corroded steel bar inside the RC has been illustrated along with a method to determine steel weight loss via digital image processing of X-ray photograms. The following conclusions can be drawn based on the experimental results:

(1) A method to visualize a corroded bar through digital image processing of X-ray photograms has been established.
(2) X-ray photograms taken from different viewing angles can be used to determine the steel weight loss of a corroded steel bar inside of concrete.
(3) The distribution of steel weight loss along a steel bar is spatially non-uniform, and the non-uniform degree of steel weight loss significantly increases with the increase of the mean steel weight loss.
(4) Maximum *SW* occurs at locations near to the stirrups, and its location varies as the mean steel weight loss increases.

It is possible that a relationship between steel weight loss and corrosion-induced surface cracks can be established. However, further experimentation with extensive study of more parameters including the effects of corroded stirrups on longitudinal steel bars will be needed to determine this relationship.

REFERENCES

[1] Andrade, C., Alonso, C., & Molina, F. J.," Cover cracking as a function of rebar corrosion: part2--numerical model," Materials and Structures, Vol. 26, 1993, pp. 532-548.

[2] Otsuki, N., Miyazato, S.-I., Diola, N., & Suzuki, H.," Influences of bending crack and water-cement ratio on chloride-induced corrosion of main reinforcing bars and stirrups," ACI Material Journal, Vol. 97, 2000, pp. 454-464.

[3] Akiyama, M., Frangopol, D. M., & Yoshia, I.," Time-dependent reliability analysis of existing RC structures in marine environment using hazard associated with airborne chlorides," Engineering Structures, Vol. 32, 2010, pp. 3768-3779.

[4] Beck, M., Goebbels, J., Burkert, A., Isecke, B., & Babler, R.," Monitoring of corrosion processes in chloride contaminated mortar by electrochemical measurement and X-ray tomography," Matrials and Corrosion, Vol. 61, 2010, pp. 475-479.

[5] Akiyama, M., and Frangopol, D.M.," Estimation of steel weight loss due to corrosion in RC members based on digital image processing of X-ray photogram," Proceedings of the Third International Symposium on Life-Cycle Civil Engineering, IALCCE2012, Vienna, Austria, October 3-6 2012; pp. 389.